A Cytoplasm-Specific Fluorescent Ligand for Selective Imaging of *RNA* G-Quadruplexes in Live Cancer Cells

Bo-Xin Zheng,[a] Wei Long,[a,b] Meng-Ting She,[c] Yakun Wang,[b] Dong Zhao,[d] Jie Yu,[a] Alan Siu-Lun Leung,[a] Ka Hin Chan,[a] Jinqiang Hou,[d] Yu-Jing Lu,*[c] and Wing-Leung Wong*[a],[b]

[a] B.-X. Zheng, Dr. W. Long, J. Yu, Dr. A.S.-L. Leung, K. H. Chan, Dr. W.-L. Wong
State Key Laboratory of Chemical Biology and Drug Discovery, Department of Applied Biology and Chemical Technology
The Hong Kong Polytechnic University
Hung Hom, Kowloon, Hong Kong SAR, China.
E-mail: wing.leung.wong@polyu.edu.hk
https://www.polyu.edu.hk/abct/people/academic-staff/dr-wong-wing-leung/

[b] Dr. W. Long, Y. Wang, Dr. W.-L. Wong
The Hong Kong Polytechnic University Shenzhen Research Institute
Shenzhen 518057, P. R. China.

[c] M.-T. She, Prof. Dr. Y.-J. Lu
School of Biomedical and Pharmaceutical Sciences
Guangdong University of Technology
Guangzhou 510006, P. R. China.
E-mail: luyj@gdut.edu.cn

[d] D. Zhao, Dr. J. Hou
Department of Chemistry, Lakehead University and Thunder Bay Regional Health Research Institute,
980 Oliver Road, Thunder Bay, ON P7B 6V4, Canada.

Abstract

The development of site-specific, target-selective and biocompatible small molecule ligands as a fluorescent tool for real-time study of cellular functions of *RNA* G-quadruplexes (G4s), which are associated with human cancers, is of significance in cancer biology. We report a fluorescent ligand that is a cytoplasm-specific and *RNA* G4-selective fluorescent biosensor in live HeLa cells. The *in vitro* results show that the ligand is highly selective targeting *RNA* G4s including *VEGF*, *NRAS*, *BCL2* and *TERRA*. These G4s are recognized as human cancer hallmarks. Moreover, intracellular competition studies with BRACO19 and PDS, and the colocalization study with G4-specific antibody (BG4) in HeLa cells may support that the ligand is highly selective binding to G4s *in cellulo*. Furthermore, the ligand was demonstrated for the first time in the visualization and monitoring of dynamic resolving process of *RNA* G4s by the overexpressed RFP-tagged DHX36 helicase in live HeLa cells.

Introduction

The guanine(G)-rich *RNA* sequence, similar to that of *DNA*, is found capable of folding into stable noncanonical secondary structures that are usually termed G-quadruplexes (G4s).[1] Despite G4s of *RNA* and *DNA* share a common motif of square planar G-quartet (or G-tetrad) moiety, one of the key structural differences found is that *RNA* G4s are usually more stable than that of *DNA* and almost exclusively adopt a parallel conformation.[2] It is because the 2'-hydroxyl group of the ribose locks the *RNA* in an anti-conformation and all strands of the G4-structure have the same directionality that favours parallel topology. Bioinformatic analyses and reporter gene-based expression assays reveal that the 5'-untranslated regions (UTRs) of human mRNAs contain putative G4-forming sequences.[3] These *RNA* G4s are found associated with translational repression of many mRNAs including cancer hallmarks, such as *MYC*, *NRAS*, *BCL2*, *VEGF* and *TRF2* that harbour G4s.[4] In addition to 5'-UTRs, 3'-UTR,[5] open reading frames (ORFs),[6] and the telomeric repeat–containing *RNA* (*TERRA*, transcribed from the human C-rich telomeric *DNA*)[7] also contain G-rich sequences that putatively form G4-structures.

Accumulating *in vitro* and *in vivo* evidences suggest that *RNA* G4s are implicated in regulating the expression of many genes that are associated with human diseases such as cancers, neurodegenerative disorders, development defects and immune deficiency.[1, 3-4] Therefore, *RNA* G4s are recognized as emerging drug targets against different diseases.[4b, 8] Currently, the intracellular G4s can be visualized and studied specifically with G4-specific antibodies such as BG4;[9] however, antibody is only limited for utilizing in fixed and permeabilized cells. To investigate the cellular function of G4s in live cells without impairing the morphological integrity of the live cells is still challenging.[1, 10] The development of cell permeable, target-selective and photostable fluorescent ligands is thus critically important to provide a convenient and selective chemical tool for imaging and monitoring of the *in vivo* formation *RNA* G4s and the resolving process that may involve enzymatic activities. Recently, the folding of *RNA* G4s has been demonstrated in human cells [1, 7, 9c] although the G4 species may just exist transiently *in vivo*.[11] Currently, a number of fluorescent ligands binding to *DNA* G4s have been reported.[12] Among these ligands, **SQgl**,[13] **CAS-C1**,[14] **CQ4**,[15] **2a**,[16] and **c_{ex}-NDI**[17] were found selectively recognizing the parallel *DNA* G4s over other topologies. Fluorescent ligands **4b**[18] and **9Cl**[19] are capable of recognizing *c-MYC DNA* G4-structures selectively. In addition, **MitoISCH**[20] and **4b**[21] were found to specifically recognize the mitochondrial G-quadruplex *DNA*. Nonetheless, with respect to literature, only few *RNA* G4-selective fluorescent ligands, such as **QUMA-1**,[22] **N-TASQ**,[23] **CyT**,[24] **V-P1**,[25] and **BEDO-3**[26], have been reported thus far. More importantly, most reported *RNA* G4-ligands are not site-selective. The ligands stain *RNA* G4s both in cytoplasm, nucleus and/or nucleoli. In the present study, we report a fluorescent *RNA* G4-ligand (**BYBX**) that has a structural design to

achieve high target-selectivity and stains *RNA* G4s located in the cytoplasm in live HeLa cells. The ligand at low concentration (2 μM) was found highly emissive for intracellular staining targeting *RNA* G4s with almost no background signal and showed robust photostability (> 1 h) under the irradiation condition (λ_{ex} = 447 nm). In addition, the cytotoxicity of the ligand against human cancer cells (HeLa, MDA-MB-231, HCT116, IC_{50} > 53 μM) and noncancerous cells (HFF1, IC_{50} > 100 μM) is very low. It is thus an excellent fluorescent biosensor of *RNA* G4s for cell imaging and monitoring in live cells with minimum interruption of normal cellular activity. Furthermore, the real-time visualization of resolving *RNA* G4s with a RFP-tagged helicase, DHX36 (a known *RNA* G4-resolving enzyme with high affinity), in live HeLa cells was demonstrated for the first time in the present study.[27] Our results reveal that **BYBX** is cytoplasm-specific in live cells and is also selectively imaged the *RNA* G4s including the cancer hallmarks of *VEGF*, *NRAS*, *BCL2* and *TERRA* in live HeLa cells.[4b]

Results and Discussion

Design of Fluorescent Ligand Selectively Targeting *RNA* G4s and Specifically Localizing in Cytoplasm in Live Cells

We previously developed a target-specific probe (**BZT-Indolium**) for fluorescence discrimination and imaging of *DNA* G4s in live human cells.[28] We found that the ligand integrated with a benzothiazole and an indolium scaffold via a rigid but freely rotatable methylene bridge is highly nuclear membrane permeable. This small cationic ligand was found only localized in nucleus and selectively bound to oncogene promoter *DNA* G4s including *c-MYC*, *BCL2*, *KRAS*, *HRAS* and *VEGF*, while the telomeric G4s were much less favourable to interact with the ligand. The observation may indicate that this cationic ligand may showed discrimination ability against different types of G4s. More importantly, we found that the ligand only exhibited very weak interaction with most non-G4 nucleic acid substrates including *DNA* and *RNA*. We thus speculated that further functionalization of the molecular structure of the ligand may alter its cellular location preference from nucleus to cytoplasm. Thus, the ligand is able to interact specifically with the cytoplasmic G4s in live cells rather than those located in nucleus. This property of molecular probe is significant because the cytoplasm-specific fluorescent probe is rarely reported in literature. We thus re-designed the ligand by modifying the substituent group at the positively charged nitrogen atom of the benzo-indolyl ring. Interestingly, we find that the structural modification for G4-ligand design at this site is very uncommon. Most reported pyridinium- or indolium-based G4-ligands are found bearing a methyl group (-CH_3) at the positively charged nitrogen atom.[29] We found that, through the integration of a polar acetamide group (-CH_2CONH_2) to substitute the non-polar methyl group at the site of the nitrogen atom at the benzo-

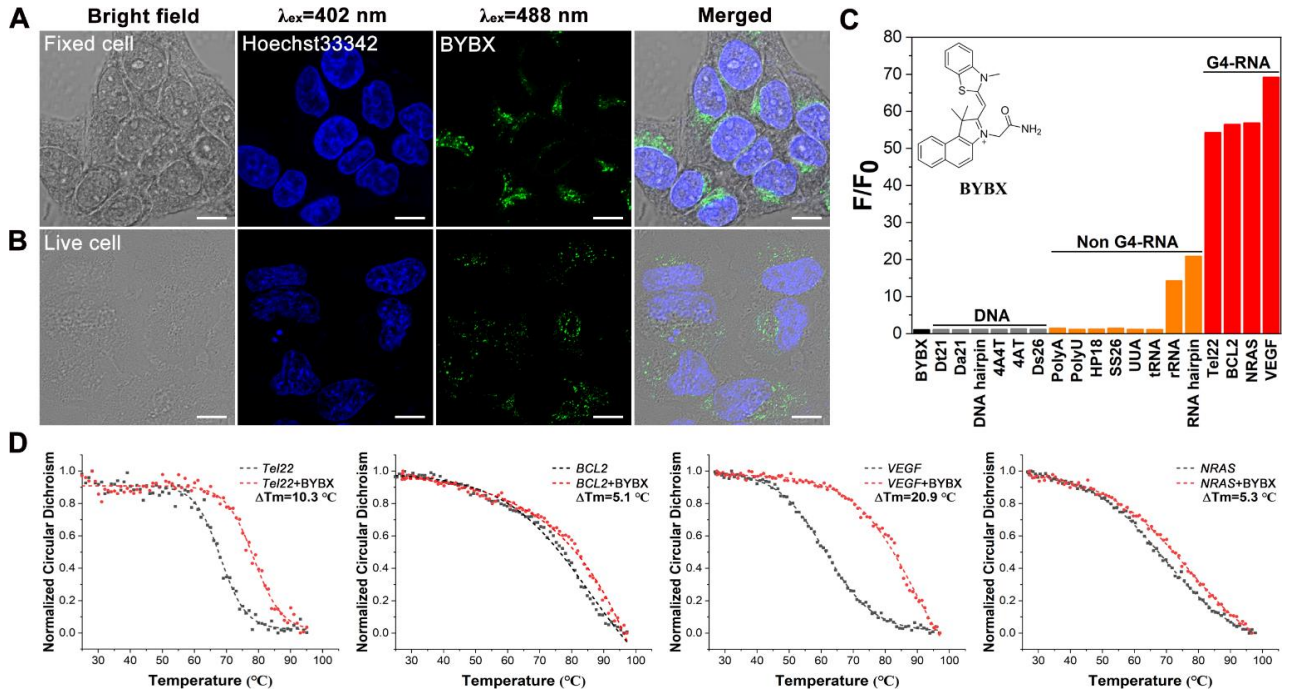

Figure 1. (A) Fluorescence images of fixed HeLa cells stained with 2 μM **BYBX** for 1 h and 1 μM Hoechst33342 for 30 min. Scale bar is 10 μm. (B) Fluorescence images of live HeLa cells stained with 2 μM **BYBX** for 1 h and 1 μM Hoechst33342 for 30 min. (C) The fluorescence intensity of **BYBX** in sensing with different nucleic acids: single-stranded *DNA*: *Dt21*, *Da21*; duplex *DNA*: *DNA hairpin*, *4A4T*, *4AT*, *Ds26*; single-stranded *RNA*: *PolyA*, *PolyU*, *SS26*; duplex *RNA*: *HP18*, *RNA hairpin*; Triplex *RNA*: *UUA*; *rRNA*; *tRNA*; *RNA* G-quadruplex: *Tel22*, *BCL2*, *VEGF*, *NRAS* in a Tris-HCl buffer (10 mM, pH 7.4) containing 60 mM KCl. The fluorescence signal was measured at 25 °C. The concentration of **BYBX** was 1 μM. (D) Normalized CD signal of G4-*RNAs* during the melting process. The concentrations of **BYBX** and G4-*RNAs* were 10 μmol and 5 μmol, respectively.

indole scaffold, a small molecule ligand (**BYBX**) was exclusively concentrated in the cytoplasm but not entering the nucleus in both live and fixed HeLa cells (Figure 1 A-B). In addition, **BYBX** exhibits excellent *RNA* G4-selective toward *VEGF*, *NRAS*, *BCL2* and *TERRA in vitro* (Figure 1 C and Figure S4). These *RNA* G4-targets are well-known important cancer hallmarks and are of great significance in cancer biology and drug discovery.[4b] Furthermore, even increasing the concentration of **BYBX** from 1 to 20 μM in live cell staining assays, the ligand is still completely localized in cytoplasm without any nuclear staining found in the cells (Figure S5). The co-localization study of **BYBX** with LAMP1 antibody (cytoplasm specific), also showed that **BYBX** is mainly located in cytoplasm (Figure S6). These results may suggest that **BYBX** is a cytoplasm-specific fluorescent ligand and can be utilized for staining and imaging the cytoplasmic *RNA* G4s specifically in live cell.

The spectroscopic property of **BYBX** was investigated with UV-Vis and fluorescence titrations for its *in vitro* interactions with various nucleic acid substrates (Table S1 and Figure S7-S8). The results are summarized in Table S2-S3 and Figure S9-S11. The fluorescence signals (λ_{ex} = 447 nm, λ_{em} = 538 nm) were found markedly enhanced when **BYBX** was interacted with *RNA* G4 substrates of *VEGF*, *NRAS*, *BCL2* and *TERRA* (54-70 folds enhancement). The substrates of rRNA and *RNA* hairpin showed mild

Table 1. The binding parameters were obtained from isothermal titration calorimetry (ITC) study for the compound **BYBX** interacting with nucleic acids.

	Tel22	*BCL2*	*VEGF*	*NRAS*	*RNA hairpin*	*rRNA*	*HP18*	*Ds26*
F/F_0 [a]	54.24	56.50	69.19	56.84	20.83	14.18	1.16	1.14
K_{eq} (μM) [b]	1.24	3.19	3.20	6.98	0.87	0.64	n.d.	n.d.
K_D (μM) [c]	3.02	2.49	2.86	3.34	12.3	12.6	18.3	14.4
N (sites) [d]	1.16	1.40	1.42	1.05	1.67	0.95	3.00	1.75
Job Plot binding ratio	2.3	1.5	1.5	1.5	-	-	-	-
ΔT_m (°C)	10.3	5.1	20.9	5.3	-0.6	-0.7	0.1	0.05

[a] The fold of fluorescent enhancement when **BYBX** and oligonucleotides were used at 1.0 μM and 2.3 μM, respectively. [b] Equilibrium binding constant of **BYBX** with oligonucleotides determined with fluorescence titration at 25 °C; n.d. denoted as not determined because the ligand-oligonucleotide binding signal was too weak for estimation. [c] The dissociation constant of **BYBX** with oligonucleotides determined with ITC at 25 °C. [d] N represents the stoichiometry of Guest-Host interaction obtained in ITC experiments.

signal enhancement (14-20 folds), while the non-G4 nucleic acid substrates exhibited almost no emission under the same assay conditions (Figure 1 C). Moreover, the results obtained from UV-Vis titrations indicate the *in-situ* formation of **BYBX**-G4 adduct, which is supported by a clear redshift of the ligand absorption peak at 447 nm (Figure S11). In addition, the increased circular dichroism (CD) absorptions at 262 nm observed under the condition without K^+ ions support that the ligand may induce *RNA* G4s formation and followed interact with the G4-structure formed to generate strong fluorescence signal. Nonetheless, the ligand-G4 interaction do not cause observable topology changes (Figure S12-13). Furthermore, lifetime measurements show that **BYBX** upon interacted with *RNA* G4 substrates including *Tel22* (2.5 ns), *BCL2* (3.3 ns), *VEGF* (5.1 ns), *NRAS* (2.7 ns) generally exhibits much longer lifetime than the ligand alone (0.1 ns) in a Tris-HCl buffer solution (Figure S10), which may further support the *in-situ* interaction of **BYBX** with *RNA* G4s.[30] The binding stoichiometry of the **BYBX**-G4 complex formed *in-situ*, estimated by Job plot analysis, was found mostly to be 1:2 and 1:1.5 (Figure S14), which were comparable with those determined with isothermal titration calorimetry (ITC) analysis (Figure S15 and Table 1). These results indicate that the binding pocket of these *RNA* G4s may accommodate one or two ligands.

The molecular docking study predicts that **BYBX** is able to stack on the G4-structure and the interaction is mainly established by *π*-*π* stacking and hydrogen bond interactions. From Figure S16 A-B, the docking results of **BYBX** in complex with the *RNA* G4 of human *TERRA* show that the naphthalene scaffold of the ligand is able to stack onto the G-quartet via *π*-*π* stacking with the guanine residues of G11, U12 and G17. The amine group of **BYBX** also forms four hydrogen bond interactions with the carbonyl group of guanines at positions G5, G11, G17 and G23. These interactions could hold **BYBX** in position. Moreover, two hydrogen bond interactions are formed between the carbonyl group of the ligand and the nitrogen atom of the amide group of G23 and U24. Furthermore, the OH groups of the *RNA* G4-structure establish interactions with the amine group of the ligand and effectively lock the ligand in place to maximize *π*-*π* stacking interactions.

The docking results of **BYBX** in complex with *RNA* G4 of human *BCL*-2 (Figure S16 C-D) reveal that *π*-*π* interactions are formed between the naphthalene scaffold and the loop residues A16 and C4,

rather than the G-tetrad, in the *RNA* G4 of human *BCL-2*. Moreover, two hydrogen bond interactions are formed between the carbonyl group of **BYBX** and the N atoms of the amide group of G3 and the amine group of A16. A hydrogen bond interaction is also formed between the amine group of **BYBX** and the hydroxyl group of G11. These interactions may effectively lock **BYBX** in place and maximize π-π stacking interactions.

BYBX was found highly selective binding to *RNA* G4s including *Tel22*, *BCL2*, *VEGF* and *NRAS*. We also found that the fluorescence intensity of the interaction signal was not significantly influenced by pH changes in buffer (Figure S17) and the common cellular sulfhydryl compounds (Figure S18). In addition, competition studies using 100-fold of non-G4 or G4-*DNA* nucleic acid substrates to compete with the *RNA* G4s showed only mild reduction of **BYBX**-G4 interaction signal (Figure S19). Moreover, the *in vitro* competition results indicate that the ligand is highly selective to *RNA* G4s. Furthermore, the enhanced fluorescence signal for the molecular interaction was found proportional to the concentration of *RNA* G4 substrates added in the titration. A good linear relationship with a low limit of detection (LOD), down to 2.2-6.4 nM, was obtained (Figure S20). The results reveal that **BYBX** is a highly sensitive fluorescent biosensor for *RNA* G4s recognition and sensing with good fluorescence quantum yields 0.13-0.24 (Figure S21).

The binding affinity of **BYBX** toward various *RNA* G4s was estimated by both fluorescence titration (K_{eq} = 1.2-7 μM) and ITC (K_D = 2.5-3.3 μM). The affinity obtained by both methods is found comparable (micromolar level). On the contrary, the non-G4 substrates exhibited either low or no binding affinity with the ligand. Moreover, the G4-stabilization ability of **BYBX** toward these *RNA* G4s was investigated with CD thermal denaturation assays. It was found that the *RNA* G4-structure was well stabilized upon interacting with the ligand, which was supported by the markedly increased melting points of the complex (ΔT_m = 5.1-20.9 °C) as shown in Figure 1 D. However, the non-G4 nucleic acid substrates were not able to give significantly increased ΔT_m (Figure S22: ΔT_m < 1 °C) in the assay, indicating that their interactions could be much weaker than that of *RNA* G4s. Taken together, all the *in vitro* results obtained thus far support that **BYBX** is highly selective targeting the *RNA* G4-structures tested and it also generates intensive fluorescence for the interaction. Compared to the non-G4 substrates, the *in-situ* formed **BYBX**-G4 complex can be stabilized by the ligand upon interaction.

Visualization of Cytoplasmic *RNA* G4s and Monitoring the Resolving Process by DHX36 Helicase in Live HeLa Cells

The live cell imaging performance of **BYBX** targeting the cytoplasmic *RNA* G4s was investigated in HeLa cells. We first confirmed the cellular location of **BYBX** in live HeLa cells. From Figure 1, the confocal images clearly indicate that the ligand is preferentially concentrated in cytoplasm but not in nucleus. We further colocalized **BYBX** with a number of organelle-specific dyes including mitochondria (Mito-Tracker), endoplasmic (ER-Tracker), and Golgi apparatus (Golgi-Tracker) and lysosomal (Lyso-Tracker) in live HeLa cells, respectively. From the confocal images shown in Figure 2, **BYBX** is not well-colocalized with any of these dyes. However, the co-localization study of **BYBX** with LAMP1 antibody (Figure S6) showed that they were well-colocalized in the cytoplasm of fixed HeLa cells. The results support that **BYBX** is a site-specific ligand and is primarily localized in cytoplasm but not targeting the cytoplasmic organelles examined. As a result, the interference or disruption of **BYBX** toward these organelles could be largely minimized or avoided when conducting live cell imaging and chemical biology study with the ligand. It could be particularly useful for targeting the cytoplasmic *RNA* G4s in live cells.

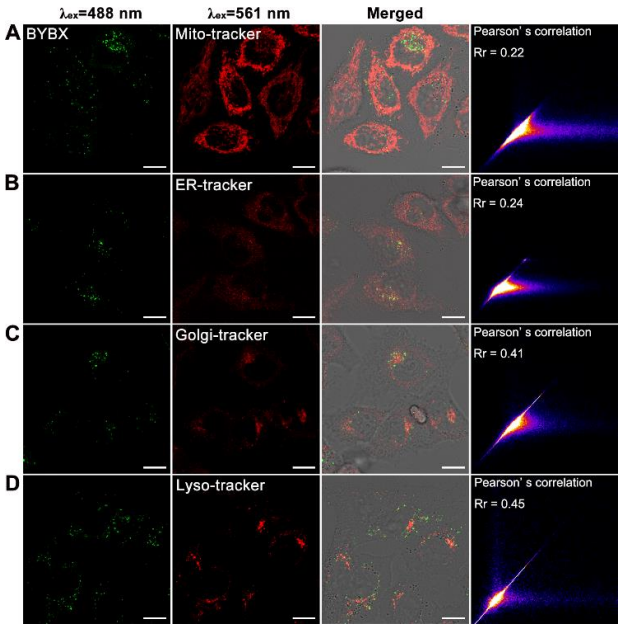

Figure 2. (A) Confocal images of live HeLa cells stained with 2 μM **BYBX** (λ_{ex} = 488 nm) for 1 h and 200 nM Mito-Tracker (red, λ_{ex} = 561 nm) for 30 min. (B) Confocal images of live HeLa cells stained with 2 μM **BYBX** (λ_{ex} = 488 nm) for 1 h and 1 μM ER-Tracker (λ_{ex} = 561 nm) for 30 min. (C) Confocal images of live HeLa cells stained with 2 μM **BYBX** (λ_{ex} = 488 nm) for 1 h and 5 μM Golgi-Tracker (λ_{ex} = 561 nm) for 30 min. (D) Confocal images of live HeLa cells stained with 2 μM **BYBX** (λ_{ex} = 488 nm) for 1 h and 1 μM Lyso-Tracker (λ_{ex} = 561 nm) for 30 min. The scale bar is 10 μm.

To verify the intracellular substrate stained by **BYBX** in live HeLa cells is *RNA*, enzymatic digestion assays were performed. After DNase I treatment (Figure 3 A), the green fluorescent foci of **BYBX** staining in HeLa cells remained intact, indicating that the ligand did not bind to *DNA* substrates. However, after RNase A treatment (Figure 3 B), the green foci were disappeared, which revealed that **BYBX** was primarily interacted with *RNA* substrates in live cells. In addition, to further verify the nature of these *RNA* substrates stained by **BYBX**, CX5461,[31] an RNA polymerase I inhibitor, was utilized to treat the cells in order to inhibit the RNA polymerase I-driven transcription of rRNA. The confocal images (Figure 3 C) showed that intensive green foci were still observed, suggesting that **BYBX** did not primarily bind to rRNA in the cells. When RNA polymerase II inhibitor, *α*-Amanitin,[32] was applied to

inhibit the transcription of mRNA in the cells, it was found that the green foci were completely disappeared (Figure 3 D). The results clearly support that **BYBX** primarily binds to mRNA substrates in live HeLa cells.

To investigate whether the identity of mRNA substrates interacted with **BYBX** in live HeLa cells was G4-structure, we performed a number of intracellular competition assays with the well-known G4-selective ligands including BRACO19[21, 33] and PDS[34] in live HeLa cells. We also conducted colocalization study using **BYBX** and a G4-specific antibody (BG4) in fixed HeLa cells. From Figure 4 B-C, compared with the control experiment shown in Figure 4 A, the green foci of the **BYBX**-mRNA adduct in cytoplasm were almost completely disappeared after the treatment with BRACO19 and PDS, respectively. It is attributed to the addition of G4-competitors, BRACO19 and PDS, that effective substitute **BYBX** from *RNA* G4s substrates. These results clearly support that BRACO19, PDS and **BYBX** may compete the same cellular substrates, which most likely are G4s. Moreover, the real-time live cell competition study of **BYBX** with BRACO19 was recorded in a video (**Video 1**). It showed evidently that the green foci in live HeLa cells were faded out gradually after the addition of BRACO19 to the cells, due to the competition for G4s.

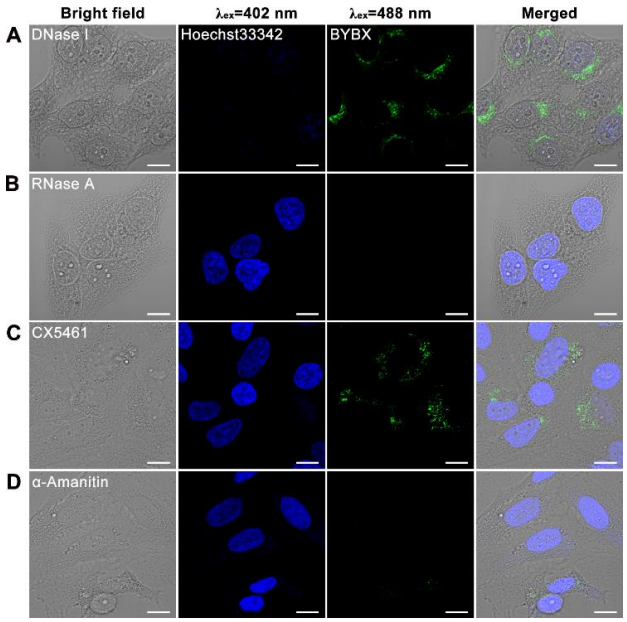

Figure 3. (A) Confocal images of fixed HeLa cells stained with 2 μM **BYBX** for 1 h and 1 μM Hoechst33342 for 30 min after DNase Ⅰ was treated for 3 h. (B) Confocal images of fixed HeLa cells stained with 2 μM **BYBX** for 1 h and 1 μM Hoechst33342 for 30 min after RNase A treated for 3 h. (C) RNA polymerase inhibitors treatments. HeLa cells were cultured in 2 μM CX5461 for 24 h before staining; confocal images of live HeLa cells stained with 2 μM **BYBX** for 1 h and 1 μM Hoechst33342 for 30 min. (D) RNA polymerase inhibitors treatments. HeLa cells were cultured in 10 μM α-Amanitin for 24 h before staining, and confocal images of live HeLa cells were stained with 2 μM **BYBX** for 1 h and 1 μM Hoechst33342 for 30 min. The scale bar is 10 μm. Quantification results analysed by Image J for the cell imaging were shown in Figure S23.

In addition, **BYBX** used in the competition assays with RNA G4s of *BLC2*, *VEGF* and *NRAS* as the substrate was titrated with BRACO19 in a buffer solution. It was found that the intensity of the fluorescence signal was reduced markedly with the increase of BRACO19 concentration, which demonstrated that the **BYBX** bound to the *RNA* G4s was substituted by the BRACO19 added (Figure S25). Furthermore, we used dimethyl sulfate (DMS) to methylate the guanines at the N7 position of nucleic acid strands in live HeLa cells. Consequently, G4-strcutres were not able to form in the cells. Thus, the cells stained with **BYBX** showed no any green fluorescence foci (Figure 4 D). We also used chemical denaturant formamide and DMS to destroy the *RNA* secondary structures *in vitro*, including

the *RNA* G4 substrates of *Tel22*, *BCL2*, *VEGF* and *NRAS* (Figure S26). The results show clearly that the green fluorescence signal of **BYBX** is markedly reduced because the mRNA sequences after the formamide and DMS treatment cannot form G4-structures to interact with the ligand.

To further elucidate the nature of the cellular *RNA* substrates interacted with **BYBX** in cytoplasm in live HeLa cells, we employed RNase III, RNase H, and RNase T1 to cleave the double-stranded *RNA*, *RNA* in *RNA*:*DNA* hybrids, and single-stranded *RNA*, respectively (Figure S27-S28). In these enzymatic treatments, both RNase III and RNase H exhibited no reduction effects on the green foci stained by **BYBX** in the cells (Figure S27 B-C), indicating that the ligand did not bind to the double-stranded *RNA* and *RNA*:*DNA* hybrids. However, when the cells were treated with RNase T1, which was an endonuclease specifically cleaving sing-stranded *RNA* at guanosine residues but not *DNA*, the green foci in HeLa cells were found disappeared completely (Figure S27 D). The results support that **BYBX** may selectively interact with the single-stranded *RNA* in cells and that most likely forms G4-structures *in cellulo*. Then, these *RNA* G4s interact with **BYBX** to generate fluorescence signal. To obtain more evidence that G4s are the binding target of **BYBX** in HeLa cells, BG4 was utilized to colocalize with the ligand in HeLa cells. Prior conducting these assays, we confirmed the specificity of BG4 by both the staining assays and EMSA assays with different nucleic acid substrates including *Da21* (single-strand *DNA*), *Ds26* (double-strand *DNA*), *ckit2* (G-quadruplex *DNA*) and *NRAS* (G-quadruplex *RNA*). The results verified that the BG4 antibody targeted specifically the *DNA* and *RNA* G-quadruplex (Figure S29). The result of these immunofluorescence assays was shown in Figure 5 A. Some green foci (**BYBX**) were found colocalized with the red staining (BG4) in HeLa cells, which may indicate that **BYBX** could possibly bind to G4-targets in the cells.

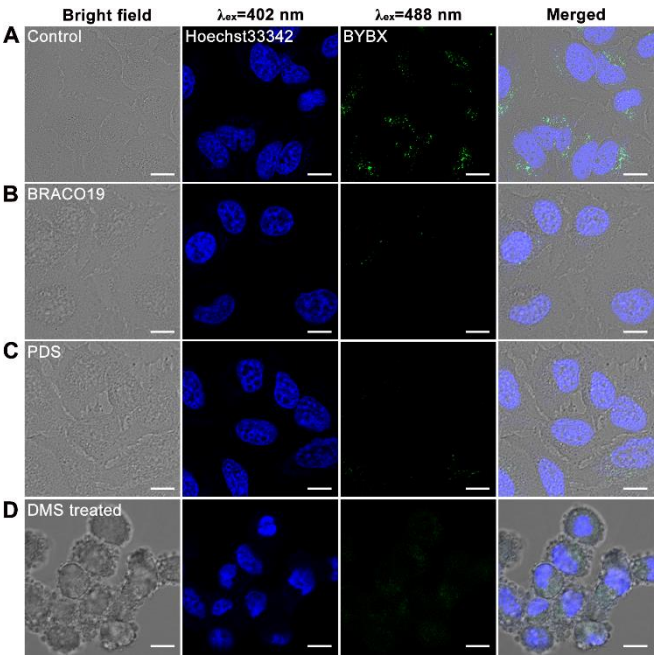

Figure 4. (A) Confocal images of live HeLa cells stained with 2 μM **BYBX** for 1 h and 1 μM Hoechst33342 for 30 min. (B) Confocal images of live HeLa cells stained with 2 μM **BYBX** for 1 h, 5 μM BRACO19 for 1 h and 1 μM Hoechst33342 for 30 min. (C) Confocal images of live HeLa cells stained with 2 μM **BYBX** for 1 h, 5 μM PDS for 1 h and 1 μM Hoechst33342 for 30 min. (D) Confocal images of live HeLa cells pre-treated with 20 mM dimethyl sulfate (DMS), 2 μM **BYBX** for 1 h and 1 μM Hoechst 33342 for 30 min. The scale bar is 10 μm. Quantification results analysed by Image J for the cell imaging were shown in Figure S24.

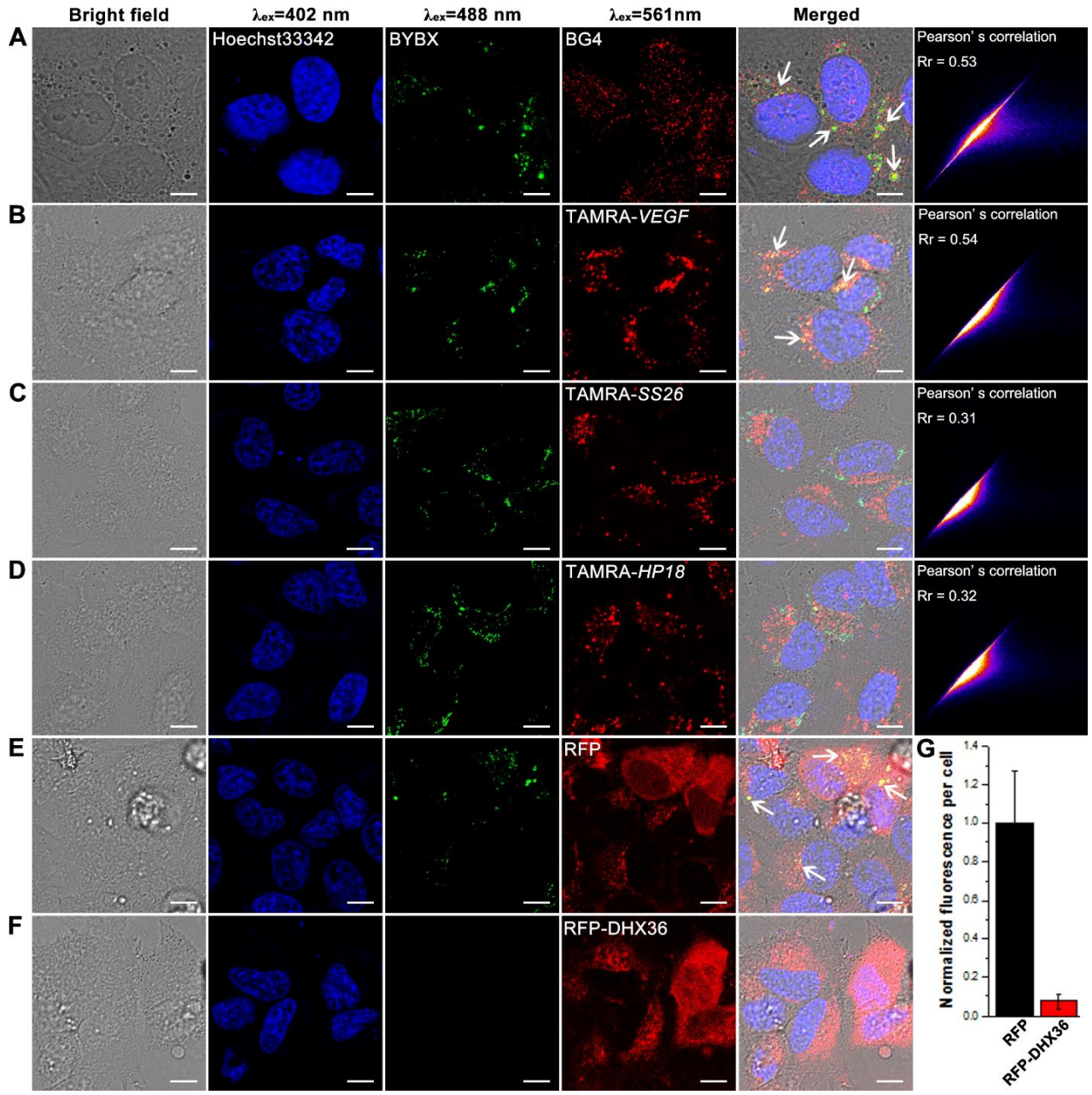

Figure 5. (A) Confocal images of fixed HeLa cells stained with 5 μM **BYBX** for 1 h, 1 μM Hoechst33342 for 30 min and G4-specific antibody BG4. The number of BG4 was quantified in Figure S30. (B) Confocal images of live HeLa cells transfected with TAMRA-*VEGF RNA* G-quadruplex for 24 h and then stained with 2 μM **BYBX** for 1 h and 1 μM Hoechst33342 for 30 min. (C) Confocal images of live HeLa cells transfected with TAMRA-*SS26* single-stranded *RNA* for 24 h and then stained with 2 μM **BYBX** for 1 h and 1 μM Hoechst33342 for 30 min. (D) Confocal images of live HeLa cells transfected with TAMRA-*HP18* duplex *RNA* for 24 h and then stained with 2 μM **BYBX** for 1 h and 1 μM Hoechst33342 for 30 min. (E) Confocal images of live HeLa cells with overexpression of RFP were stained with 2 μM **BYBX** for 1 h and 1 μM Hoechst33342 for 30 min. (F) Confocal images of live HeLa cells with overexpression of RFP-tagged G4-specific RNA helicase DHX36 were stained with 2 μM **BYBX** for 1 h and 1 μM Hoechst33342 for 30 min. (G) Quantification results of (E) and (F). The scale bar is 10 μm.

We also transfected different TAMRA-labelled *RNA* substrates including TAMRA-labelled pre-folded *RNA* G-quadruplex (TAMRA-*VEGF*), single-stranded *RNA* (TAMRA-*SS26*) and duplex *RNA* (TAMRA-*HP18*) into live HeLa cells, respectively. Then, we investigated the intracellular interaction of labelled substrates with **BYBX** in live cells. From Figure 5 B, the transfected TAMRA-*VEGF* was found well-

colocalized with **BYBX** in different cells, while TAMRA-*SS26* and TAMRA-*HP18* did not show obvious colocalization (Figure 5 C-D). The results suggest that **BYBX** is highly selective targeting *RNA* G4s *in cellulo*.

DHX36 is an RNA helicase and resolves G4-structures and it has high specificity and affinity toward *RNA* G4s.[35] To further verify the intracellular binding target of **BYBX** could be *RNA* G4s, we thus overexpressed RFP-tagged DHX36 helicase in live HeLa cells and followed to monitor the fluorescent changes of green foci stained by **BYBX** in live cells. In the control experiment, we found that RFP (red fluorescent protein) was also overexpressed in the cells and a number of the green foci were observed clearly. It is because RFP does not resolve the G4s stained by **BYBX** (Figure 5 E). However, when the cells overexpressed RFP-tagged DHX36, the green foci were gradually cleared away and finally disappeared completely after 12 h (Figure 5 F and Figure 6) because the *RNA* G4s were resolved by the overexpressed RFP-tagged DHX36 (red fluorescence) in the cells. The monitoring of RFP-tagged DHX36 expression and the resolving of *RNA* G4s in live HeLa cells were recorded in a video (**Video 2**). It shows evidently that the intracellular green foci disappear over time and this is probably because the *RNA* G4s are being resolved in cytoplasm of live HeLa cells, which is mostly like attributed to the activity of DHX36 that resolves *RNA* G4s *in cellulo*. Taken together, all these results obtained support that **BYBX** is located in cytoplasm and selectively interacts with *RNA* G4s there in live cells.

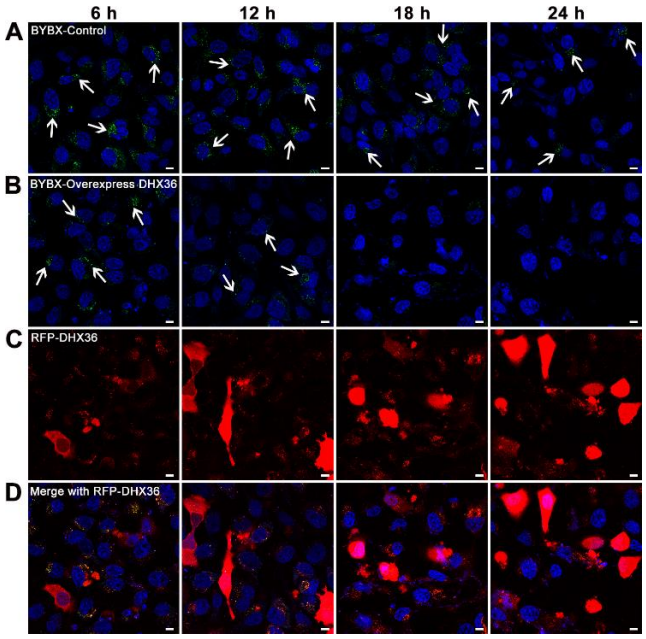

Figure 6. (A) Confocal images of live HeLa cells stained with 2 μM **BYBX** for 1 h, and then the cells were photographed at the 6 h, the 12 h, the 18 h and the 24 h respectively. (B) Confocal images of live HeLa cells stained with 2 μM **BYBX** for 1 h and then were transfected with RFP-tagged G-quadruplex specific RNA helicase DHX36, and then the cells were photographed at the 6 h, the 12 h, the 18 h and the 24 h respectively. The excitation of **BYBX** and RFP-DHX36 was 488 nm. (C) Live HeLa cells were transfected with RFP-tagged G-quadruplex specific RNA helicase DHX36, and then the cells were photographed at the 6 h, the 12 h, the 18 h and the 24 h respectively. The excitation of RFP-DHX36 was 561 nm. (D) The merged image of (B) and (C). The cell nucleus was indicated by Hoechst33342. The cell nucleus was stained by Hoechst33342 (blue). The scale bar is 10 μm.

To visualize and monitor the real-time cellular location of *RNA* G4s in live cells are of significance for chemical biology investigations to understand their biofunctions.[36] Because **BYBX** is highly selective binding to *RNA* G4s in cytoplasm, we thus attempt to demonstrate its ability to visualize the real-time location and the formation and resolving of *RNA* G4s in live cells. In the *in vitro* study, we have

demonstrated that, when **BYBX** interacts with *RNA* G4s, it generates intensive green fluorescence signal. The green foci observed *in celluo* may indicate that *RNA* G4s could be probably formed at the site. On the other hand, when the green fluorescence signal at the site is faded gradually or disappeared, it may indicate that the G4s formed could be resolved by enzymes. We therefore attempted to utilize **BYBX** as a target-selective fluorescent tool for real-time monitoring and visualizing the formation and resolving process of *RNA* G4s located in cytoplasm of live HeLa cells. In the experiment, HeLa cells were incubated with **BYBX** and then confocal images were recorded as shown Figure 7. The blue stained area by Hoechst33342 in the cells is the nucleus. Moreover, four sites in live HeLa cells stained by **BYBX** (green foci) were selected for monitoring real-time changes of the green fluorescence signal (Figure 7: regions 1-4, marked with a red box). The changes were then recorded real-time under a confocal microscope. The images of these selected regions were enlarged for comparison and presented with a time interval of 10 s continuously for 90 s (Figure S31). From the time-lapse images recorded, it is clear to observe that the intensity of the green fluorescent staining in these regions is kept changing, which may indicate that a dynamic process of forming and resolving *RNA* G4s for certain cellular activity is ongoing at the site.

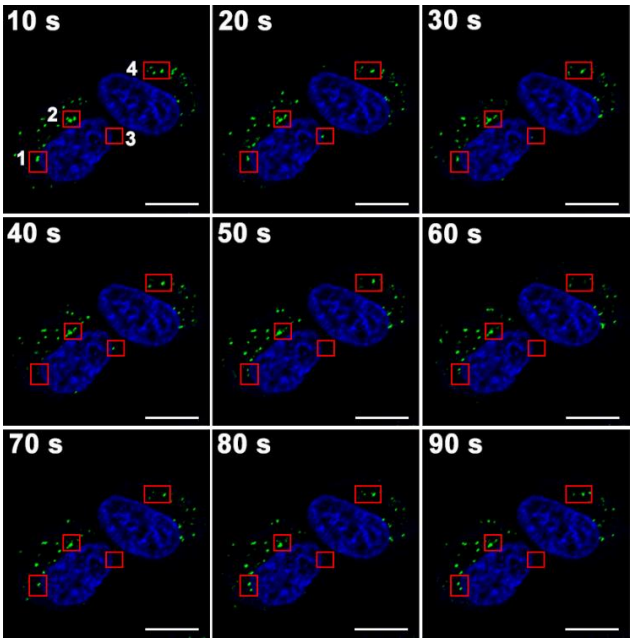

Figure 7. Time-lapse imaging of G4-*RNA* dynamics using **BYBX** (2 μM, λ_{ex} = 488 nm, green) in live HeLa cells. The cell nucleus was stained by Hoechst33342 (blue). The scale bar is 10 μm.

Intracellular Photostability and Cytotoxicity of BYBX for Live Imaging and Monitoring Targeting *RNA* G4s

In order to demonstrate the fluorescence intensity changes of the green foci observed in live HeLa cells showed in Figure 6 and Figure 7 were not due to the photobleaching of **BYBX**, the photostability of the ligand was investigated. We found that **BYBX** exhibited excellent photostability against photobleaching, as demonstrated in Figure 8 A, a steady and intensive fluorescence signal for **BYBX** interacting with *RNA* G4s was maintained continuously without any significant reduction over 60 min under the irradiation at the excitation wavelength (447 nm). Moreover, in the live cell imaging, the green foci of **BYBX** in live HeLa cells were also kept steady over 60 min under the excitation wavelength at 488 nm (Figure 8 B and **Video 3**). These results clearly support that **BYBX** is robust against

photobleaching and is a good fluorescent probe selectively targeting *RNA* G4s in cytoplasm for live cell imaging and real-time monitoring. This small molecule ligand may be particularly useful for the experiments requiring long investigation time in live cells.

In addition, the fluorescent probe with low cytotoxicity against live cells may largely reduce or minimize the adverse effects that may interrupt the normal cellular functions during the real-time investigation. The cytotoxicity of **BYBX** was thus evaluated against a number of human cancer cell lines including HeLa, HCT116 and MDA-MB-231 and a non-cancerous cell line (HFF1) by MTT assays. The results were shown in Figure S32. The IC_{50} values were summarized in Table S4. In general, **BYBX** exhibits low toxicity against all these human cell lines tested. The IC_{50} for HCT116 and HFF1 were found greater than 100 μM while for HeLa and MDA-MB-231 were found about 53.9 μM and 72.2 μM, respectively. Nonetheless, in the present study, the concentration of **BYBX** used in live cell staining and imaging is only 2 μM. The ligand under this concentration shows almost no cytotoxicity against all the human cells tested and offers strong fluorescence signal targeting the *RNA* G4s in cytoplasm.

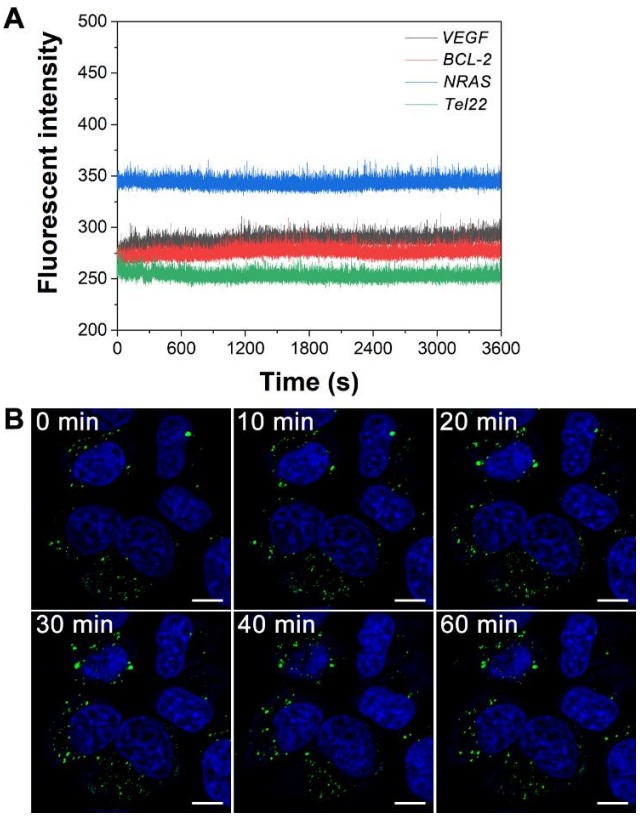

Figure 8. Photostability study. (A) The change of fluorescence signal responses of **BYBX** (1 μM) with different *RNA* G4s at 1 μM (*VEGF*, *BCL2*, *NRAS* and *Tel22*) for a period of 0 to 3600 s in a Tris-HCl buffer solution (10 mM, pH 7.4, containing 60 mM KCl); λ_{ex} = 447 nm. (B) The time-lapse imaging in live HeLa cells with **BYBX** (2 μM) in 1 h; λ_{ex} = 488 nm. The scale bar is 10 μm.

Furthermore, the results of apoptosis analysis performed with flow cytometry show that **BYBX** at the concentrations of 0-40 μM do not cause significant apoptosis in HeLa cells (Figure S33: 0.3%-2.1%). The ligand (0-40 μM) incubated with HeLa cells for 24 h also showed almost no effect on cell cycle disorder (Figure S34). Taken together, **BYBX** was demonstrated to be a sensitive fluorescent biosensor and selectively targeting *RNA* G4s in cytoplasm with excellent biocompatibility and photostability for real-time imaging and tracking of *RNA* G4s in live human cells.

Conclusion

A fluorescent ligand (**BYBX**) was synthesized through the integration of a benzothiazole and a benzoindolium scaffold with a rigid but rotatable methylene bridge. The ligand showed almost no background fluorescence signal both in buffer solution and *in cellulo* conditions. Moreover, the ligand was found to be site-specific in live cells. It specifically localizes in cytoplasm but not entering nucleus in live cells. The ligand was also demonstrated to be an *RNA* G4-selective biosensor with excellent sensitivity, biocompatibility and photostability for real-time imaging and tracking of *RNA* G4 formation and resolving in live cells. The *in vitro* experimental results showed that **BYBX** selectively interacted with the *RNA* G4s of the human cancer hallmarks including *VEGF*, *NRAS*, *BCL2* and *TERRA* against the non-G4 *DNA* and *RNA* substrates. In addition, the intracellular results revealed that the ligand selectively imaging *RNA* G4s in both fixed and live HeLa cells. Furthermore, the ligand was demonstrated for the first time to visualize and monitor the real-time resolving process of *RNA* G4s by the overexpressed RFP-tagged DHX36 helicase in live HeLa cells. This cytoplasm-specific and non-toxic small molecule ligand may provide a useful and target-selective fluorescent tool for real-time study of cellular function of *RNA* G4s associated with the cancer hallmarks in cancer biology and drug discovery.

Experimental Section

The detailed synthetic procedures and full characterization data for ligand **BYBX**, the experimental methods and conditions for *in vitro* assays and cell imaging, and the molecular docking study are given in the Supporting Information.

Acknowledgements

The work is fully supported by the grant recieved from the Research Grants Council of the Hong Kong Special Administrative Region, China (RGC Project No. 15300522). W.L acknowledges the award of a postdoctoral fellowship administered by the Research Committee of The Hong Kong Polytechnic University. The University Research Facilities on Life Sciences and Chemical and Environmental Analysis of The Hong Kong Polytechnic University are also acknowledged.

Keywords: DHX36 • Fluorescent G4-ligand • G4-structure resolving • Live cell imaging • *RNA* G-quadruplex

References

[1] L. Dumas, P. Herviou, E. Dassi, A. Cammas, S. Millevoi, *Trends Biochem. Sci.* **2021**, *46*, 270-283.

[2] P. Kharel, G. Becker, V. Tsvetkov, P. Ivanov, *Nucleic Acids Res.* **2020**, *48*, 12534-12555.

[3] A. Bugaut, S. Balasubramanian, *Nucleic Acids Res.* **2012**, *40*, 4727-4741.
[4] a) D. Varshney, J. Spiegel, K. Zyner, D. Tannahill, S. Balasubramanian, *Nat. Rev. Mol. Cell Biol.* **2020**, *21*, 459-474; b) A. Cammas, S. Millevoi, *Nucleic Acids Res.* **2017**, *45*, 1584-1595.
[5] D. S. Lee, L. R. Ghanem, Y. Barash, *Nat. Commun.* **2020**, *11*, 1-12.
[6] P. Murat, G. Marsico, B. Herdy, A. Ghanbarian, G. Portella, S. Balasubramanian, *Genome Biol.* **2018**, *19*, 1-24.
[7] D. Müller, I. Bessi, C. Richter, H. Schwalbe, *Angew. Chem. Int. Ed.* **2021**, *60*, 10895-10901.
[8] a) P. Kharel, S. Balaratnam, N. Beals, S. Basu, *Wiley Interdiscip. Rev.: RNA* **2020**, *11*, e1568; b) J. Xu, H. Huang, X. Zhou, *JACS Au* **2021**, *1*, 2146-2161; c) B. Zheng, J. Yu, W. Long, K. H. Chan, A. S.-L. Leung, W.-L. Wong, *Chem. Commun.* **2023**, *59*, 1415-1433.
[9] a) G. Biffi, D. Tannahill, J. McCafferty, S. Balasubramanian, *Nat. Chem.* **2013**, *5*, 182-186; b) S. M. Javadekar, N. M. Nilavar, A. Paranjape, K. Das, S. C. Raghavan, *DNA Res.* **2020**, *27*, dsaa024; c) G. Biffi, M. Di Antonio, D. Tannahill, S. Balasubramanian, *Nat. Chem.* **2014**, *6*, 75-80.
[10] a) F. Raguseo, S. Chowdhury, A. Minard, M. Di Antonio, *Chem. Commun.* **2020**, *56*, 1317-1324; b) Y. Dai, X. Teng, J. Li, *Angew. Chem. Int. Ed.* **2022**, *61*, e202111132.
[11] J. U. Guo, D. P. Bartel, *Science* **2016**, *353*, aaf5371.
[12] a) B. R. Vummidi, J. Alzeer, N. W. Luedtke, *ChemBioChem* **2013**, *14*, 540-558; b) R. Paul, D. Dutta, T. Das, M. Debnath, J. Dash, *Chem. Eur. J.* **2021**, *27*, 8590-8599; c) B. Prasad, M. Doimo, M. Andréasson, V. L'Hôte, E. Chorell, S. Wanrooij, *Chem. Sci.* **2022**, *13*, 2347-2354.
[13] V. Grande, F. Doria, M. Freccero, F. Würthner, *Angew. Chem. Int. Ed.* **2017**, *56*, 7520-7524.
[14] V. Grande, C.-A. Shen, M. Deiana, M. Dudek, J. Olesiak-Banska, K. Matczyszyn, F. Würthner, *Chem. Sci.* **2018**, *9*, 8375-8381.
[15] M. Deiana, K. Chand, J. Jamroskovic, I. Obi, E. Chorell, N. Sabouri, *Angew. Chem. Int. Ed.* **2020**, *59*, 896-902.
[16] M. Deiana, I. Obi, M. Andreasson, S. Tamilselvi, K. Chand, E. Chorell, N. Sabouri, *ACS Chem. Biol.* **2021**, *16*, 1365-1376.
[17] M. Zuffo, A. Guédin, E.-D. Leriche, F. Doria, V. Pirota, V. Gabelica, J.-L. Mergny, M. Freccero, *Nucleic Acids Res.* **2018**, *46*, e115-e115.
[18] M. Deiana, K. Chand, J. Jamroskovic, R. N. Das, I. Obi, E. Chorell, N. Sabouri, *Nanoscale* **2020**, *12*, 12950-12957.
[19] Q. Zhai, C. Gao, J. Ding, Y. Zhang, B. Islam, W. Lan, H. Hou, H. Deng, J. Li, Z. Hu, H. I. Mohamed, S. Xu, C. Cao, S. M. Haider, D. Wei, *Nucleic Acids Res.* **2019**, *47*, 2190-2204.
[20] X.-C. Chen, G.-X. Tang, W.-H. Luo, W. Shao, J. Dai, S.-T. Zeng, Z.-S. Huang, S.-B. Chen, J.-H. Tan, *J. Am. Chem. Soc.* **2021**, *143*, 20779-20791.
[21] M. Deiana, K. Chand, E. Chorell, N. Sabouri, *J. Phys. Chem. Lett.* **2023**, *14*, 1862-1869.
[22] X. C. Chen, S. B. Chen, J. Dai, J. H. Yuan, T. M. Ou, Z. S. Huang, J. H. Tan, *Angew. Chem. Int. Ed.* **2018**, *130*, 4792-4796.
[23] A. l. Laguerre, K. Hukezalie, P. Winckler, F. Katranji, G. t. Chanteloup, M. Pirrotta, J.-M. Perrier-Cornet, J. M. Wong, D. Monchaud, *J. Am. Chem. Soc.* **2015**, *137*, 8521-8525.
[24] S. Xu, Q. Li, J. Xiang, Q. Yang, H. Sun, A. Guan, L. Wang, Y. Liu, L. Yu, Y. Shi, *Nucleic Acids Res.* **2015**, *43*, 9575-9586.
[25] L. Yu, P. Verwilst, I. Shim, Y.-Q. Zhao, Y. Zhou, J. S. Kim, *CCS Chem.* **2021**, *3*, 2725-2739.
[26] Z.-Y. Yu, W.-H. Luo, X.-C. Chen, S.-B. Chen, Z.-S. Huang, J.-H. Tan, *Sens. Actuators, B* **2020**, *324*, 128770.
[27] M. C. Chen, R. Tippana, N. A. Demeshkina, P. Murat, S. Balasubramanian, S. Myong, A. R. Ferré-D'Amaré, *Nature* **2018**, *558*, 465-469.

[28] B.-X. Zheng, M.-T. She, W. Long, Y.-Y. Xu, Y.-H. Zhang, X.-H. Huang, W. Liu, J.-Q. Hou, W.-L. Wong, Y.-J. Lu, *Chem. Commun.* **2020**, *56*, 15016-15019.

[29] A. R. Duarte, E. Cadoni, A. S. Ressurreição, R. Moreira, A. Paulo, *ChemMedChem* **2018**, *13*, 869-893.

[30] A. Shivalingam, M. Izquierdo, A. L. Marois, A. Vyšniauskas, K. Suhling, M. K. Kuimova, R. Vilar, *Nat. Commun.* **2015**, *6*, 1-10.

[31] D. Drygin, A. Lin, J. Bliesath, C. B. Ho, S. E. O'Brien, C. Proffitt, M. Omori, M. Haddach, M. K. Schwaebe, A. Siddiqui-Jain, N. Streiner, J. E. Quin, E. Sanij, M. J. Bywater, R. D. Hannan, D. Ryckman, K. Anderes, W. G. Rice, *Cancer Res.* **2011**, *71*, 1418-1430.

[32] M. W. Park, H. S. Lee, E. Y. Kim, K. A. Lee, *Dev. Reprod.* **2013**, *17*, 63-72.

[33] a) A. M. Burger, F. Dai, C. M. Schultes, A. P. Reszka, M. J. Moore, J. A. Double, S. Neidle, *Cancer Res.* **2005**, *65*, 1489-1496; b) M.-T. She, J.-W. Yang, B.-X. Zheng, W. Long, X.-H. Huang, J.-R. Luo, Z.-X. Chen, A.-L. Liu, D.-P. Cai, W.-L. Wong, Y.-J. Lu, *Chem. Eng. J.* **2022**, *446*, 136947; c) M. Deiana, J. Jamroskovic, I. Obi, N. Sabouri, *Chem. Commun.* **2020**, *56*, 14251-14254; d) M. Deiana, M. Mosser, T. Le Bahers, E. Dumont, M. Dudek, S. Denis-Quanquin, N. Sabouri, C. Andraud, K. Matczyszyn, C. Monnereau, L. Guy, *Nanoscale* **2021**, *13*, 13795-13808.

[34] D. Koirala, S. Dhakal, B. Ashbridge, Y. Sannohe, R. Rodriguez, H. Sugiyama, S. Balasubramanian, H. Mao, *Nat. Chem.* **2011**, *3*, 782-787.

[35] E. Booy, M. Meier, N. Okun, S. Novakowski, S. Xiong, J. Stetefeld, S. McKenna, *Nucleic Acids Res.* **2012**, *40*, 4110-4124.

[36] a) K. Lyu, S.-B. Chen, C.-Y. Chan, J.-H. Tan, C. K. Kwok, *Chem. Sci.* **2019**, *10*, 11095-11102; b) Y. Tao, Y. Zheng, Q. Zhai, D. Wei, *Bioorg. Chem.* **2021**, *110*, 104804.